Predictions of Global Sea Surface Temperature Anomalies: Introduction of CWB/OPGSST1.1 Forecast System

Shu-Ping Weng[1], Yea-Ching Tung[2], and Wen-Hao Huang[2]

1: National Taiwan Normal University, 2: Central Weather Bureau

Abstract

Skillful prediction of SST a few seasons in advance is essential for the success of two-tier forecast system to make seasonal climate prediction. The newly developed global SST prediction system at CWB, OPGSST1.1, an optimized combination of dynamical and statistical forecast modules using superensemble technique, is introduced in this report.

Prediction skills of OPGSST1.1 in different time scales are verified to be comparable with those of other systems. Particularly, the spring predictability barrier (SPB) of ENSO forecasting is largely reduced after ensembling two statistical predictors: upper ocean heat content anomalies (OHCA) in the tropical Pacific and sea level pressure anomalies (SLPA) over the Philippine Sea into the system. The former substantiates the delayed oscillator paradigm that the memory of ENSO dynamics is mainly stored in the subsurface thermocline depth displacement, and the latter demonstrates the importance of SLPA in the western north Pacific as the precursor to the ENSO turnabout. Prediction skills of warm and cold SST conditions around the globe are also discussed.

Keywords: climate prediction, superensemble, ocean heat content, thermocline, SPB

1. Introduction

One of the major tasks of the ongoing climate prediction project at CWB is to establish the two-tier climate prediction system with a 7-month lead time. Proposed by Bengtsson et al. (1993), it predicts future atmospheric conditions using an AGCM alone forced by pre-forecasted SSTs. In this approach, the prediction skill depends on several factors. First, it works for the most important forcing (Equatorial Pacific SST) and for those regions where SST determines the local wind convergence while SST itself is primarily determined by ocean processes, but it has limited capability where atmospheric forcing play a major feedback to the ocean (Wang et al. 2004, 2005). Second, it depends on the accuracy of the pre-predicted global SST, which provides the major boundary forcing to drive the stand alone AGCM. Third, it depends on the capability of AGCM in catching the predictable part of atmospheric variability possibly. This report focuses on the second issue.

2. OPGSST1.1 prediction system

The CWB/OPGSST system is designed in a flexible way to combine multi-SST predictions from both dynamic and statistical modules to make an ensemble forecast. The flexibility is reserved in the sense that the system serves as a template that can easily takes new prediction made by other centers/methods into account as long as their prediction skills have been verified. The complete document concerning the physical consideration, configuration, procedure, and data sources of CWB/OPGSST system is described in Weng et al. (2004a).

Theoretical works and diagnostic studies have suggested that ocean subsurface thermocline adjustment plays a central role in the ENSO dynamics. The subsurface temperature signals and upper ocean heat content (UOHC), an integrated measure of the thermocline displacement, often provide useful precursory signals for ocean mixed layer (or sea surface) temperature prediction. This is especially true when the predicted time scale becomes increasing longer. Indeed, the establishment of zonal-mean UOHC anomaly in the equatorial Pacific sector several seasons in advance has been found by many diagnostic studies (e.g. McPhaden 2003) and coupled model simulations (e.g. An and Kang 2000) to be an indicative of the onset and demise of ENSO episodes. Impacts of ENSO event have been recognized as the most important source to the changes of global climate system in the interannual timescale. Skillful prediction of forthcoming ENSO episodes provided by the underlying thermocline displacement is thus desired.

Potential skill improvements by using UOHC in the tropical Pacific (hereafter TPOHC) as predictors for regional as well as global SSTA predictions have been suggested by Weng et al. (2004b). Recently, efforts have been made to upgrade OPGSST system from version 1.0 to 1.1 by incorporating the SST predictions generated by TPOHC predictors. In the following, the performances of OPGSST1.1 are examined by running the system in the hindcast mode ("take-one-out" Jackknife cross-validation) to produce *future* 7-month GSSTA predictions.

3. Prediction skill of GSST anomalies

Fig.1 shows the 6-month lead NINO3.4 index predicted by the OPGSST1.1 (dashed lines). Superimposed are the observations (solid lines), consensus predictions (CONS, simple averaging of all modules), and the predictions made by individual modules labeled in the bottom as ICM2A (Intermediate Coupled Model version 2A), ICM2B (Intermediate Coupled Model version 2B), PER (damped persistent forecast), NINOP6F7 (use past 6-month SSTA in the NINO3.4 domain as predictors), PSLP3F1 (use past 3-month SLPA in the Philippine Sea as predictors), and TPOHC (use past 6-month TPOHC as predictors). Although individual model shows different degree of deviations, predicted evolution of NINO3.4 SSTA by the OPGSST1.1 closely follows the observations. In fact, simple consensus averaging, which assigns equal weight to each prediction, already showed good skill for the ENSO predictions. The OPGSST1.1 using multi-model superensemble method (MMSE, Krishnamurti et al. 1999), which assigns optimized weight to individual module based on its past skill performance, further improves the skill as the lead time becomes increasing longer. Nevertheless, the phasing of major ENSO episodes is found to be slightly delayed (1～3 months) as compared with the observations. Compared with statistical models, both dynamic ICM2A and ICM2B model predictions are also found to have larger bias in current OPGSST system.

Spatial distributions of forecasted skills represented by pattern correlation (PC) and root-mean-square-error (RMSE) are shown in the left and right panels of Fig.2, respectively. Skillful SSTA predictions with high PC values and low RMSE are found to mainly locate within the 20° tropical band. As lead time increases from 3-month to 6-month, prediction skills are further restricted over the central tropical Pacific, central Indian Ocean, and northwestern Pacific. Simultaneously, the RMSE increases rapidly in the eastern tropical Pacific cold tongue and the storm track regions of mid-latitudes. To further quantify the local prediction skills, the Taylor diagrams for 8 key regions over the tropical warm oceans are shown in Fig.3 where the normalized RMSE, i.e., the RMSE scaled by the observed standard deviation, is given by the radial distance and the correlation coefficient between the observed and predicted SST anomalies is given by the cosine of the azimuthal angle. Making it simpler, only the lead time equals to 1, 3, 5, and 7 months are marked. First, skills of OPGSST1.1 are found to surpass any individual module after optimization. Second, skill of current system heavily relies on the statistical modules particularly for the long lead predictions. Assimilating the predictions made by TPOHC predictors tends to improve the long-lead skill in most areas. Dynamical modules primarily make their contributions to the short lead (1～3 months) predictions of SSTA over the NINO3 and NINO1+2 regions. Third, the skills decay rapidly after 3- month lead over the NINO1+2 and tropical western Pacific (TWPC) regions as no model shows ability to capture the future SST evolution.

4. Season-dependent skill variability

Impacts of TPOHC predictors on the long-lead prediction skills of OPGSST1.1 are demonstrated in Fig.4a where the season dependent skill variability of 6-month lead ENSO prediction, portrayed by the anomaly correlation of NINO3.4 index, are shown for the PERSI, OPGSST1.0, TPOHC, and OPGSST1.1. The well-known SPB is clearly shown in the PERSI model (open circle): the prediction skills drop dramatically when passing the northern spring season. Although a better result was obtained through the MMSE procedure, the SPB still exists in the previous OPGSST1.0 (solid circle). In the new OPGSST1.1 (solid square), it is the contributions of TPOHC predictors (open square) that largely reduce the SPB problem as suggested by McPhaden (2003) recently.

It should mention that the impacts of TPOHC predictors are not always positive elsewhere. Fig.4b shows the season-dependent skill variability in the South China Sea (SCS) over which the so-called fall predictability barrier (FPB) exists; the prediction skill of PERSI model decreases while passing the northern fall season. Incorporating the TPOHC predictions even make it worse. Over this domain, it is mainly the NINOP6F7 model (plus labels) prediction that tends to remedy the FPB problem.

Fig.5 examines the global perspective of the season-dependent skill variability where the 6-month lead PCs of standard DJF, MAM, JJA, and SON seasons are shown in the left and right panels for PERSI and OPGSST1.1 predictions, respectively. From DJF (JJA) to JJA (DJF), reductions of prediction skill in the PERSI are evident in the central-to-eastern tropical Pacific (southern-to-eastern Asian monsoon oceans) originated from the western coasts of Peru (southern Japan). These predictability barriers are largely overcome in the OPGSST1.1; 6-month lead PC in the central-to-eastern tropical Pacific during JJA seasons is raised from below 0.2 in the PERSI (Fig.5c) to above 0.6 in the OPGSST1.1 (Fig.5g), and 6-month lead pattern correlation in the Asian monsoon oceans during DJF seasons is also raised from below 0.4 in the PERSI (Fig.5a) to above 0.6 at best in the OPGSST1.1 (Fig.5e). Prediction skills elsewhere are also improved demonstrating the power of MMSE method.

In addition to the post-processing procedure, the major contributors to the improvements of SPB are found to be both TPOHC and PSLP3F1 (Fig.6). Although the latter is only secondary, it can affect the final ENSO prediction skill while monitoring the NINO3.4 index. Seasonality of the forecast skill has been the subject of active research. Our results indicate that *the predictability barrier exist the choice of robust subsurface predictors that can substantially overcome this barrier.*

Fig.7 shows the scatter plots of observed against forecasted SSTA for 6-month lead JJA seasons in the NINO3.4 (upper panels), and DJF seasons in the SCS (lower panels) domains. For the PERSI (Figs.7a and 7c), the skills are close to the white noise distributions of predicted versus the observed SST anomalies. Although the best linear fit lines (Figs. 7b and 7d) demonstrate that the prediction skills for the SPB in the NINO3.4 and FPB in the SCS domains are improved, the OPGSST1.1 tends to underestimate the observed extremes. This might be due to limitation of linear regression method.

5. Interannual skill variability

Observations and 6-month lead ensemble predictions for the major ENSO episodes are shown in Fig.8 where the x-axis corresponds to the DJF mean of the indicated years and the y-axis indicates the ensemble predictions for forecasts initialized during the preceding JJA. Although the sign of the anomaly is well captured in almost all the cases, individual model in general underestimates the observed amplitude. There is also indication that the models perform better and more consistent during the El Niño warm events but spread wider during the La Niña cold events. Nevertheless, the OPGSST prediction tends to remedy for individual model toward the observed magnitude.

Results of Fig.8 illustrate that current system can predict the phase of ENSO with some extent of accuracy at least two-season ahead. This is further explored in Fig.9 where the hit rate versus false alarm rate plots of warm, normal, and cold terciles are shown for 3- and 6-month lead ENSO predictions among model members. The hit (false alarm) rate for different category is defined as ratio of the total number of forecasted events belonging to the specific category divided by the number of times it was really observed (not observed). Note that the hit rate and false alarm rate must be examined together to prevent the so-called "crying wolf" problem and the model prediction is usually considered as skillful when the hit rate is larger than the false alarm rate.

Both warm and cold terciles express higher hit rates and lower false alarm rates as compared with those in the normal tercile. The OPGSST system tries to optimize the final predictions by raising the hit rate and at the same time keeping the false alarm rate as low as possible in all three categories. On the other hand, although the simple averaging consensus prediction (solid square symbols) works reasonably well for the warm tercile, it does not work well for the cold tercile as individual members show large inconsistence as compared with that for the warm tercile. Additional aspects are noted when increasing the lead time. First, the prediction skill also lost the most in the normal tercile as the hit rate (false alarm rate) decreases (increases) rapidly. Moreover, the dynamical models seem to have troubles in keeping the skillful predictions. Second, it is found that the maintenance of skill in the cold tercile is largely contributed by the TPOHC model in maintaining the high hit rate. In the warm tercile, however, it seems that the NINOP6F7 model contributes the most in the final OPGSST prediction.

We also calculated the hit rate as well as false alarm rate of 6-month lead optimized predictions for every grid point around the globe as shown in Fig.10. Comparing with the others, warm tercile (upper panel) is found to have higher hit rate in the tropical Indo-Pacific with centers locating in the central Indian Ocean, subtropical northwestern Pacific, and off-equatorial central Pacific to the south. Secondary high hit rates of local warm SSTA prediction are also found in the coast regions of west Australia, eastern South America, and eastern Canada. On the other hand, higher hit rates of cold tercile (bottom panel) are mainly restricted within the Pacific Ocean basin with centers locating in the central Pacific east of dateline, New Zealand Isl., and northern Pacific north of Hawaii Isl. One thing interesting is that the skillful cold SSTA predictions are almost absent around the Asian-Australian monsoon oceans. The normal tercile (middle panel) is found to have the worst hit rate from the global viewpoint. Higher hit rates are only limited to those ocean regions west of Peru.

References

An, S.-I., and B. Wang, 2000: Interdecadal change of the structure of ENSO mode and its impact on the ENSO frequency. *J. Climate*, **13**, 2044-2055.

An, S.-I., and I.-S. Kang, 2000: A further investigation of the recharge oscillator paradigm for ENSO using a simple coupled model with the zonal mean and eddy separated. *J. Climate,* **13**, 1987-1993.

Bengtsson, L., U. Schlese, E. Roeckner, M. Latif, T.P. Barnett and N.Graham, 1993: A two-tiered approach to long-range climate forecasting, *Science,* **261**, 1026-1029.

Krishnamurti, T.N., C. M. Kishtawal, LaRow, E. Timothy, D. R. Bachiochi, Z. Zhang, E. C. Williford, S. Gadgil, and S. Surendran, 1999: Improved Weather and Seasonal Climate Forecasts from Multimodel Superensemble. *Science* **285**, 1548-1550.

McPhaden, M. J., 2003: Tropical Pacific Ocean heat content variations and ENSO persistence barriers. *Geophysical Research Letters*, **30**, 1480-1483.

Wang, B., 1995: Interdecadal changes in El Nino onset in the last four decades. *J. Climate*, **8**, 267-258.

Wang, B., X. Fu, Q. Ding, I.-S. Kang, K. Jin, J. Shukla, and F. Doblas-Reyes, 2005: Challenges in prediction of summer monsoon rainfall: Inadequacy of the tier two system, submitted to *J. Climate.*

Weng, S.-P., B. Wang, W.-H.Huang, 2004a: 中央氣象局全球海溫預報校驗系統, Tech. Report No. IEI-C93-CFM-DWR-014.

Weng, S.-P., B. Wang, W.-H.Huang, 2004b: 印度洋與西北太平洋海溫預報方法之改進, Tech. Report No. IEI-C93-CFM-DWR-015.

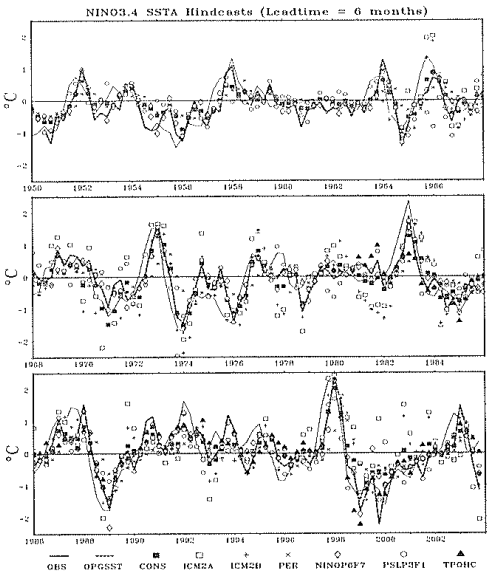

Figure 1 The observed (solid lines) and predicted monthly-mean SST anomalies with 6-month lead time in the CWB/OPGSST system (dashed lines) over the NINO3.4 domain (170° W-to-120° W; 5° S-to-5° N) during 54-year period of 1950-to-2003. Inside the figure, the predictions made by individual model involved in the system as well as the consensus (i.e. simple averaging) prediction are also marked by different labels at months of January, April, July, and October.

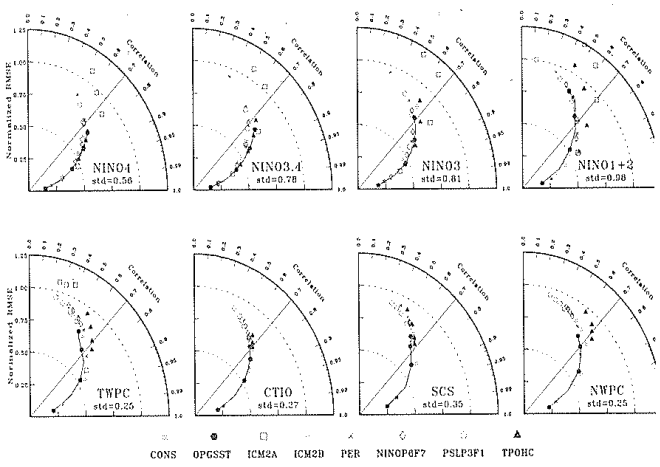

Figure 3 Taylor diagrams of the normalized RMSE and correlation coefficients between observed and predicted SST anomalies (with lead time = 1, 3, 5, 7 months) for consensus (yellow squares), optimized (red dots), and individual model in different regions: NINO4 (160° E-to-150° W; 5° S-to-5° N), NINO3.4 (170° W-to-120° W; 5° S-to-5° N), NINO3 (150° W-to-90° W; 5° S-to-5° N), NINO1+2 (90° W-to-80° W; 0° -to-10° S), (upper panels), tropical western Pacific (TWPC, 120° E-to-160° E; 5° S-to-5° N), central tropical Indian Ocean (CTIO, 60° E-to-90° E; 7.5° S-to-10° N), South China Sea (SCS, 100° E-to-120° E; 0° -to-20° N), and northwestern Pacific (NWPC, 120° E-to-160° E; 7.5° N-to-22.5° N) (lower panels).

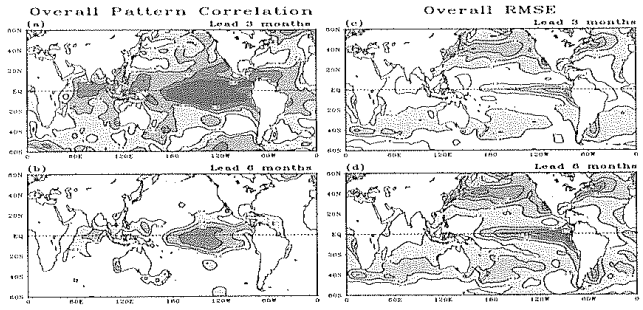

Figure 2 The overall (1950-to-2003) pattern correlation coefficients are shown for (a) lead time = 3 months and (b) lead time = 6 months. Correlations larger than (0.5, 0.7, 0.8) are (light, medium, heavy) shaded. The corresponding RMSE patterns are shown in (c) and (d), respectively. Values of RMSE larger than (0.3° , 0.4° , 0.5°) C are (light, medium, heavy) shaded.

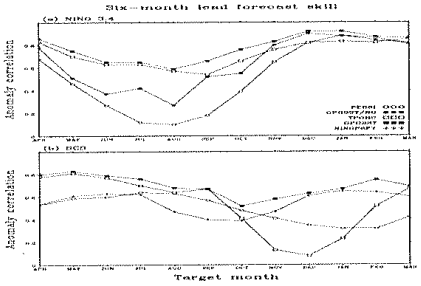

Figure 4 The forecast skills represented as temporal anomaly correlations for persistent (PERSI, open circle), OPGSST1.0 (i.e. OPGSST/NO TPOHC, solid circle), TPOHC (open square), OPGSST1.1 (solid square), and NINOP6F7 (plus label) model predictions are shown in (a) and (b) for NINO3.4 and South China Sea (SCS) domains, respectively. Note that the 12 target months, each has been with six-month lead time, start from April through the calendar year to detect the season-dependent skill variability.

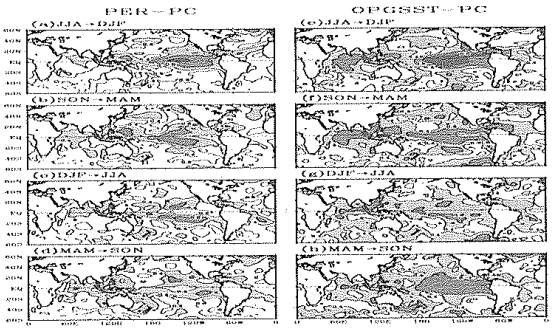

Figure 5 The six-month lead pattern correlations (PC) between observed and damped persistent [(a)-(d) in the left panels] predictions and between observed and OPGSST1.1 [(e)-(h) in the right panels] predicted global SST anomalies. To save space, only the averages of 4 standard seasons: DJF, MAM, JJA, and SON, each month is the 6-th month prediction, are shown from top to bottom. Contour interval is 0.2, values of PC larger than (0.4, 0.6, 0.8) are (light, medium, heavy) shaded.

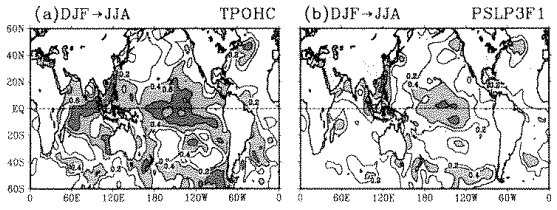

Figure 6 Same as Figure 5c or 5g, but for the results obtained by using (a) TPOHC and (b) PSLP3F1 statistical modules.

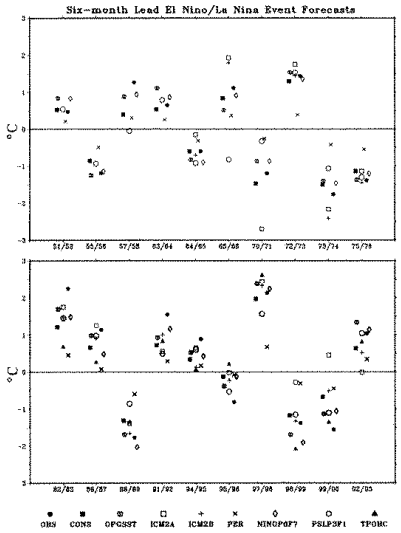

Figure 8 The observed (solid circles) and six-month lead forecasted NINO3.4 indices by consensus (solid squares) and OPGSST (open circles with bars) predictions as well as by the different members (marked by different labels shown in the bottom) for 20 major El Niño/La Niña episodes during the 1950-to-2003 period.

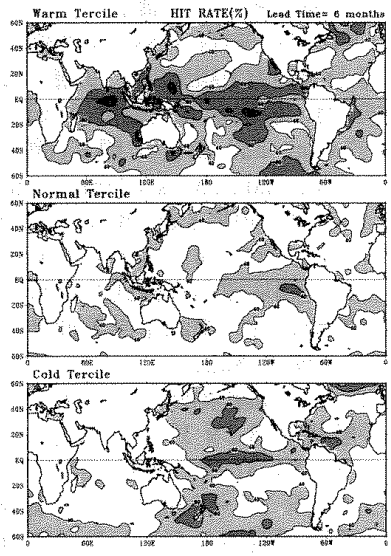

Figure 10 Spatial distributions of hit rates for warm (upper panel), normal (middle panel), and cold (lower panel) terciles when the lead time = 6 months. Contour interval is 20%; values of hit rate larger than (40, 60, 80) % are (light, medium, heavy) shaded.

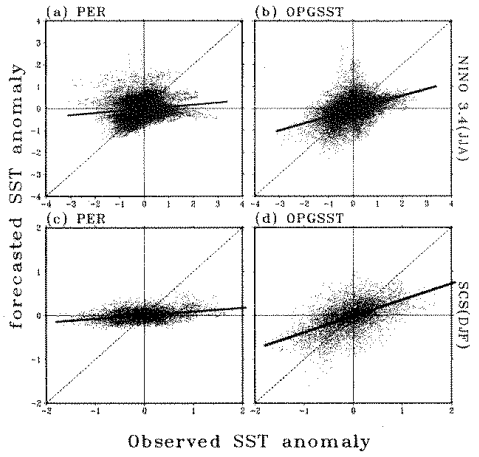

Figure 7 The scatter plots of observed (x-axis) and six-month lead forecasted SST anomalies (y-axis) for all grid points located inside the NINO3.4 domain during JJA seasons (upper panels) and for those inside the SCS domain during DJF seasons (lower panels). The (a) and (c) are the results of damped persistent predictions while the (b) and (d) are the results obtained from the OPGSST1.1 system. The best linear fits (thick solid lines) are also drawn.

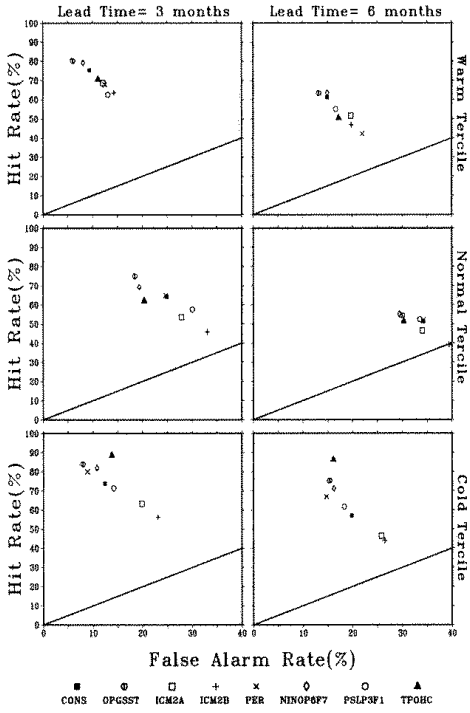

Figure 9 The hit rate (y-axis) against false alarm rate (x-axis) of warm (upper panels), normal (middle panels), and cold (lower panels) terciles of the ENSO prediction measured by the NINO3.4 index. The left and right panels are for the three-month and six-month lead time, respectively. The lines mark where the hit rate equals the false alarm rate. Different modules are marked by different labels (bottom).